Evaluation of chronically implanted subdural boron doped diamond/CNT recording electrodes in miniature swine brain

Napoleon Torres-Martinez, Celine Cretallaz, David Ratel, Pascal Mailley, Christophe Gaude, Thomas Costecalde, Clément Hebert, Philippe Bergonzo, Emmanuel Scorsone, Jean-Paul Mazellier, et al.

Evaluation of Chronically implanted Subdural Boron Doped Diamond/CNT recording electrodes in miniature swine brain

Napoleon Torres-Martinez [a], Celine Cretallaz [a], David Ratel [a], Pascal Mailley [b], Christophe Gaude [a], Thomas Costecalde [a], Clément Hebert [c], Philippe Bergonzo [c], Emmanuel Scorsone [c], Jean-Paul Mazellier [d], Jean-Louis Divoux [e], Fabien Sauter-Starace [a,*]

[a] *Univ. Grenoble Alpes, CEA, LETI, CLINATEC, MINATEC Campus, F-38000 Grenoble, France*
[b] *Univ. Grenoble Alpes, CEA, LETI, DTBS, MINATEC Campus, F-38000 Grenoble, France*
[c] *CEA, LIST, Diamond Sensors Laboratory, 91191, Gif Sur Yvette, France*
[d] *Thales Research and Technology, Route Departementale 128, Palaiseau 91767, France*
[e] *Axonic MXM, Vallauris, France*

Abstract

When implantable recording devices for brain or neural electrical activity are designed, the number of available materials for electrodes is quite limited. The material must be biocompatible with respect to ISO10993, its electrochemical properties must remain stable and the response of cells or tissues can be mitigated, especially on the glial scar. This involves electrode characterization pre- implantation and impedance spectroscopy during chronic implantation, in order to evaluate both electrode properties and performance. This study was aimed at a comparison of the long-term behavior of a nanostructured boron-doped diamond (BDD) with a nanostructured Platinum Iridium (PtIr) electrode. Firstly, a batch of cortical grids with bare and modified contacts (2mm in diameter) was engineered for implantation. Secondly a miniature swine model was developed.

This study highlighted the predominant role of electrode surface roughness on the quality of recordings. Rough PtIr contacts and BDD coated ones showed comparable behavior after three-month implantation with a slight increase of the modulus of the impedance and a tissue capsule. Nevertheless, immunohistochemistry analysis did not exhibit either a toxic or irritation reaction. With regard to biocompatibility, promising long term results are shown for both materials.

Introduction

The technical achievements presented in this paper were carried out within the framework of the European project Neurocare (FP7). This project included biologists, medical doctors, physicists and industrial partners to assess the potential of BDD as an electrode material for in-vitro or in-vivo devices (ECoG grids, cochlear and retina implants). Based on a comparison between TiN

and BDD electrode contacts, tested in subcutaneous conditions on rodents, Alcaide's analysis [1] stated that BDD electrodes elicited significantly thinner fibrous capsules and a milder inflammatory reaction at both time periods. Thus, this study may constitute an appropriate material to support stable performance of implantable neural electrodes. To our knowledge, there are very few results in the literature on BDD biocompatibility and functionality in-vivo on a larger animal. In this paper, we investigate the long-term biocompatibility and neural signal stability of the BDD electrode on a mini-swine model.

When selecting the electrode material for an active implantable device, three issues must be addressed: (a) the electrode material itself should be inert and stable (b) the mechanical strain produced by its implantation should be minimized (including secondary local molecular and cellular changes, i.e. activation of fibrosis or glial cells, loss of perfusion, secondary metabolic injury, and neuronal degeneration [2]), (c) moreover for stimulation devices, non-lesional electrical charge injection and charge density limits, should be respected to provide acute or chronic stimulation.

Regarding point (a) there are numerous normalized controls gathered in ISO10993 to assess the biocompatibility of the materials. For the particular case of intracortical recording electrodes, the introduction of a foreign body (point (b)) in the brain elicits mechanical strain, cell membrane disruption and micro-hemorrhages at the vessel network level (Blood Brain Barrier disruption). These mechanisms are revealed by bi-photon microscopy and cytokines release which has a role in the inflammatory reaction of the acute and chronic response [2]. For this study, the electrode arrays were inserted between the dura-mater and the arachnoid and triggered tissue encapsulation. Compared to Kozai's intraparenchymal conditions, the element of the microenvironment differ in quantity and in type. The thickness of the resulting glial scar impairs the electrochemical behavior of the electrode which is measurable through electrochemical impedance magnitude and phase spectra. With regard to point (c), both Merrill ([3] and Cogan [4] described the electrochemical behavior of the electrodes in-vivo (biphasic balanced stimulation, capacitive or pseudo-capacitive behavior during stimulation using metallic electrodes). They included the influence of the three dimensional structure of porous TiN electrodes within the limits of the rate of electron and ion transport. Eventually, charge and charge density injections are limited by the

electrochemical behavior of the material but also by the onset of damages at the cell level given by Shannon [5] and Mc Creery et al.[6].

Taking into account these requirements, we intended to investigate the properties of Boron Doped Diamonds (BDD) for a Multi-Electrode Arrays (MEA). This new material was also investigated by Piret et al. [7] for in-vitro neural interfacing. In this article, the authors compared impedances in PBS, signal to noise ratio and in-vitro neural recordings for flat platinum or black platinum electrode arrays (20 µm in diameter) covered by nanostructured BDD in a culture medium (platinum or black platinum provided by Qwane Biosciences. Piret et al. showed that the increase of the effective surface, related to the 3D nanostructured diamond, lessened the impedance modulus tenfold from 1 Hz to 10 kHz and hence improved the signal to noise ratio but also showed greater mechanical stability than black platinum. Previously, our group acquired similar results with implantable electrodes (30 µm in diameter) coated with Carbon NanoTubes (CNTs): these coatings decreased impedances compared to titanium nitride (TiN) contacts [8]. Moreover using a π-stacking strategy, we grafted numerous surface chemistries on CNTs. The influence of these surface chemistries on neural networks was characterized in-vitro with primary cell cultures. [9] showed that surface chemistries of CNTs mitigated the adhesion of neurons and consequently the configuration of the neural network. Unfortunately, the process of synthesis of CNTs was optimized for density and adhesion to the substrate, revealed to be inappropriate for chronic implantation because macrophages were able to remove CNTs from implanted samples.

We then sought a conductive coating resistant to mechanical and chemical aggression of macrophages, and decided to adapt the process of BDD coatings to macroscopic PtIr contacts (2 mm in diameter). A combination of BDD and CNTs appeared to be an interesting material for in-vivo electrodes for either recording or stimulation.

Diamonds have a wide electrochemical window in aqueous media and with or without chemical modification are a choice option for biosensing[10]. Its chemical stability is extremely interesting for long-term usability as contact material [11]. [12] used it to monitor neurotransmitter (dopamine) release during Deep Brain Stimulation. Diamonds are also well known for their biocompatibility properties in-vitro [13], [14], [15], [16], [17], [18], and in-vivo [19], [20].

Initially, we wanted to start from the WIMAGINE® contacts (the ECoG device developed by CEA Clinatec for Brain Computer Interfaces [21]). These electrodes are made of laminated

platinum iridium cut and embossed to obtain the so-called ‘bowl hat' shape (Fig. 1, top). The direct deposition of the diamond layer showed poor adhesion properties: the electrode surface required abrasion, sandblasting and additional tungsten deposition as an adhesion layer. For these reasons, we took advantage of parallel developments on the cochlear probe performed by our partner Axonic MXM, in which roughness is optimized thanks to a proprietary electroerosion process. The diamond layer happened to adhere on rough PtIr without any additional treatment.

Platinum iridium is classically used for cochlear or deep brain stimulation electrodes, thus we should be able to compare our BDD electrode to the gold standard of implantable devices. Consequently, for 3 months in-vivo assessments in recording conditions, we decided to build an electrode array embedding nanostructured (rough) PtIr contacts with or without nanostructured BDD in a silicone rubber grid, with a transcutaneous cable and connector. Further in-vitro assessments of the electrodes characteristics showed that the rough platinum surface have a reduced electrochemical activity attributed to Sulphur (probably Sulphur dioxide) which partially poisoned the platinum surface [22].

* Corresponding author.
E-mail address: fabien.sauter@cea.fr

1. Materials and methods

a) Manufacturing of the BDD electrodes and integration in a silicone substrate

The processing steps are shown in Schematic 1. They consists in the deposition of nanostructured BDD on disk of platinum iridium. The electrodes were diced from a rod of medical grade platinum iridium (90/10) using a proprietary electroerosion process which provides the electrodes with a roughness in the range of 1.6µm Root Mean Square (Schematic 1-1). The surface of the platinum iridium disks was coated with a 30 nm conformal layer of BDD (Schematic 1-2). The effective surface is enhanced thanks to a layer of Carbon nanotubes between the two depositions of BDD. The process is adapted from [23]. **Detailed in supplementary data.**

The doping level of the thin boron doped diamond layer was approx. $1.5x10^{21}$ cm^{-3} as determined by SIMS measurements meaning that the BDD is a metal like materials[24], [25]. As the growth process is adapted from [23], we can estimate a sp^2/sp^3 ratio in the diamond layer in the order of

1% based on Raman spectroscopy. However in the case of the nanostructured surface, which is a sandwich of BDD/ CNT/BDD, the sp^2 contribution would mainly be attributed to the CNT.

Then, the composite disks were electrically welded medical-grade insulated stainless wires without any technical difficulty. This proved the diamond coating's compatibility with processes of implantable medical devices. The electrodes were arrayed on a grid and the wires embedded in a tubing, both in medical grade silicone rubbers MED 4750 (Nusil Corp, Carpentera) and Silastic tubing (ref. 508-005, Dow Corning, Midland, Ml). The wires were eventually brazed to a Micro Plastic Circular Connectors - Type SS from Omnetics®.

The open area of each contact is about 2 mm in diameter (see Fig. 1) and a pitch of 4 mm. The overall dimensions of the MEA are the following (8 mm * 16 mm, thickness 0.7 mm).

b) Implantation of the devices

The experimental protocol was approved by ethics committee of Grenoble (N°12) and registered under the number 178_Clinatec-NTM-08 and complied with the EU directive 22nd September 2010 (2010/63/EU) on the care and use of laboratory animals.

Two Yucatan mini-pigs were premedicated and anesthetized for the implantation of the electrode arrays. Previous experiments in primate cortical implantation [26],[27] were adapted to swine anatomical features. For this in-vivo analysis, we implanted two electrode arrays over each sensorimotor cortex (see Fig. 1 and Suppl. Fig. 1) and biological controls in cortical areas that were not affected by the surgical procedure. This was done to avoid confounding surgical lesions which would have interfered with the analysis. **Detailed in supplementary data.**

c) Electrochemical Impedance Spectroscopy and cyclic voltammetry prior to implantation

The impedance and the cathodic charge storage capacity (CSC) of the electrodes was assessed by means of Electrochemical Impedance Spectroscopy (EIS) and cyclic voltammetry (CV) at room temperature in Phosphate Buffer Saline (PBS) 1X. **Detailed in supplementary data.**

d) Scanning Electron microscopy

To image the nanostructures prior and after implantation, we used a SEM and for explanted electrode arrays, samples were rinsed in PBS and dehydrated stepwise with ethanol. **Detailed in supplementary data.**

e) Electrochemical Impedance Spectroscopy follow up during implantation

To check the grid efficiency for cortical recordings, impedance spectroscopy sessions (6 contacts placed over right hemisphere and 6 in the left) were performed during 3 months after surgery. **Detailed in supplementary data.**

f) Cortical activity recording (ECoG)

Once a week, in order to compute the Power Spectrum Density (PSD), we recorded 10 min of the ECoG signals throughout an electronic board to a clinical set-up dedicated to electrophysiological recordings. **Detailed in supplementary data.**

g) Tissue preparation and histological analysis of brain reactivity

Three months after implantation, we perfused transcardially the mini-pig B with 10% Neutral Buffered Formalin to fix the tissue prior to explantation. Once the brain were frozen, we cut brain slices and applied specific stain for histological analysis. **Detailed in supplementary data.**

2. Results and discussion

a) SEM of embossed platinum iridium contacts

Whereas the nanostructures are generated by a specific dicing process based on electroerosion, our reference in terms of contact is a 3D contacts obtained by embossing of a Pt90Ir10 sheet. The roughness and structure of this sheet is qualitatively characterized using scanning electron microscopy. Based on Fig. 2, we see that the so-called bowl-hat electrode which was our reference in terms of electrochemical behavior is relatively rough. We can even distinguish the direction of the lamination at the right hand side of Fig. 2.

b) Electrochemical impedance spectroscopy characterization in PBS

In Fig. 3, we plotted the impedance modulus and phase of each contact. For comparison, we also characterized 12 contacts (2.2 mm in diameter) of flat platinum from embossed contacts (so called bowl-hat) used in the WIMAGINE® ECoG device[21]. The geometry of the three set ups are rigorously identical.

The platinum iridium impedance spectroscopy highlights very consistent behaviors. The error bars related to the standard error are limited in logarithmic scale, nevertheless range from 7.4% to 24% of the mean values. The manufacturing process was inspired from the industrial process

used for cochlear implants and resulted in limited variance, see Fig. 3-A. If we were to set up new experiments, we would increase the reference electrode surface compared to the working electrode since this can influence the high frequency behavior of the impedance.

Concerning the roughness, [7] compared BDD to platinum deposition made on polyimide or parylene reproducing the polish of the silicon substrate, our reference the bowl-hat electrode have a much higher roughness.

Obviously, the high frequency impedance is comparable, we notice a different cut-off frequency which corresponds to the shift between capacitive and ohmic behavior. Consequently, we report a reduction of the impedance modulus below 10 kHz and a shift of cut-off frequency (about 235 Hz for the Rough and 1660 Hz flat platinum respectively vs. 1000 Hz for nanostructured BDD). Nevertheless the presence of Sulphur dioxide traces may be a problem for in-vivo stimulation. Electrochemical processes to remove these adsorbed atoms may be investigated for the next generation.

The 3D nanostructuration based on carbon nanotubes described by [23] improved the performances of BDD. However, compared to a laminated and embossed platinum iridium foil, the electrochemical impedance is comparable. Significant additional improvements were associated to direct nanostructuration of the platinum iridium contacts. This is consistent with [28], who showed that electrochemical nanostructured platinum grass was preferred to black platinum in terms of adhesion and closer to iridium oxide or PEDOT in terms of charge injection.

c) Electrochemical impedance spectroscopy follow up after implantation

The Bode spectrums of Fig. 3 are the averages of the 5 contacts of each electrode array, the error bar stands for the standard error. At week 1, the impedance is quite comparable between rough platinum and BDD with a cut off frequency slightly higher for BDD. At week 12, from high frequency to 10 kHz the difference between the mean impedances is not significant. However, due to its higher roughness, the platinum contacts have a lower slope and the cut-off frequency on the EIS compared to BDD contacts, which is consistent with the EIS in PBS before implantation.

The mean impedance at 1 kHz but also 320, 150 and 10Hz are reported in Fig. 4 for each week. Based on the neurosurgeons experience, we may say that the impedance magnitude slightly decreased due to the edema around the implant immediately after surgery. Then during about 4

weeks the impedance increased, afterwards the impedance decreased and tended to stabilize. Considering the error bars, the evolution at 10Hz is not significant. These trends in impedance at 1 kHz are consistent with [29].

d) Analysis of ECoG signals

With the setup described above, we obtained at least one cortical recording a week. These data were analyzed in terms of Power Spectral Density (PSD) (Fig. 5). The functional contents of the ECoG recordings cannot be compared since the grids are not placed exactly above the same cortical areas and the animal was in idle state. At week 1, there is no significant difference between nanostructured BDD and Rough platinum contacts. Whereas at week 12, from 3Hz to 300Hz, the PSD of the BDD contacts is nearly 5dB higher than the one recorded with the platinum contacts. The footprint in the brain attributed to the MEA thickness and the stiffness of the cables was deeper for the Platinum side (Fig. 10-D), which may call this comparison into question. Additional experiments will be necessary to confirm. Nevertheless, this data suggests that the ECoG recording may be operational in the long-term, ensuring the functionality of the device.

e) SEM of contacts before implantation and after a three months long contact

Before implantation, we characterized the nanostructured BDD contacts using the SEM H-4100.

In Fig. 6-A, we clearly see on the left the edge of carbon nanotubes related to the nickel (catalyst) deposition edge and on the right, a zoom on the mixed structure of carbon nanotubes coated by BDD.

From Fig. 6-B, the bundle structure was still visible at the surface of the electrode thus asserting a good chemical and mechanical stability of the BDD coating after long term in-vivo implantation.

We proceeded the same characterizations and comparisons for rough platinum iridium contacts. Its roughness and spongy surface is highlighted in Fig. 7-C.

On Fig. 7-D, we can also report based on the picture on the right that the nanostructure has resisted to long term in-vivo conditions.

f) Cyclic voltammetry

The voltage windows shall prevent excessive cathodic current out of the electrode. Setting this limit to -20 µA, we swept the voltage from [-1.4 V, 1.4 V] for the BDD and [-0.8 V, 1 V] for platinum iridium contacts, see Fig. 8.

As expected the diamond response is nearly flat in the [-0.8 V – 1 V] window in sulfuric acid media pH 1 (Fig. 9-A) since the diamond exhibits wide electrochemical window in aqueous media [30]. By extending the electrochemical window to [-1.4 V – 1.4 V] (Fig. 11-B) in PBS 1X solution, one can see an electrochemical reduction peak at -0.8 V and a large increase of the cathodic current at -1.3 V that are respectively associated to oxygen reduction and hydrogen evolution [31]. In the anodic region, the strong oxidation current seeable at 1.3 V is associated to water hydrolysis which is concomitant to diamond surface oxidation. Thereby, during pulsing, it will be mandatory to limit the potential incursion to the window [-0.7 V – 1.1 V] to avoid any hydrolysis phenomenon. In addition, the capacitive behavior of implant contacts dedicated to electrostimulation is fundamental since it allows safe charge injection. It's important to note here that as expected BDD contacts exhibit poor capacitive response even if the roughness is strongly enhanced by the proposed architecture.

According to its electrochemical behavior, platinum contacts were characterized in the [-0.8 V – 1 V] potential window. Both, rough and flat platinum contacts voltammograms show in sulfuric acid (pH 1) a strong cathodic response at -0.6 V associated to hydrogen evolution. After inversion of the scanning direction, one can see for the flat platinum the marked reoxidation wave of adsorbed hydrogen species at -0.2 V. Conversely, for the rough contacts no significant wave is observed except an ill-defined wave between -0.2 and 0.6 V. This electrochemical wave is partially hidden by the large capacitive response of rough platinum (this capacitive response is consistent with Pt behavior in PBS as highlighted in Fig. 9-B). At pH 1 in sulfuric acid, any electrochemical response associated to the surface oxidation of platinum is seeable in the [0.5 – 1 V] window as expected.

However, considering its higher developed surface, rough platinum was supposed to interact much more than flat platinum with sulfuric acid solution leading to larger hydrogen evolution response. Fig. 9-A is contradictory with this assumption and suggests a marked difference between rough and flat platinum reactivity.

To compare the reactivity of both platinum surfaces and diamond, we performed CV characterization in ferri-ferrocyanide (4 mM in PBS 1X) used here as redox probe. Fig. 9 shows that the cyclic voltammetry behaviour of the different materials was qualitatively different. The electrochemical response of ferri-ferrocyanide is easily seen for BDD and flat platinum whereas it's absent for rough platinum. However, the recorded voltammograms exhibit poor reversibility with ΔE_p of about 250 and 450 mV respectively for BDD and flat platinum surfaces. Note that BDD [31] and platinum contacts, ferri-ferrocyanide is generally a fast and reversible redox system with peak to peak potential difference (ΔE_p) close to the theoretical value of 60 mV at 25°C. In the case of our BDD contacts, this behaviour could be explained by the poor electron exchange capacity of the diamond interface due to the synthesis conditions of the diamond layer (boron concentration, deposition temperature) that may generate sp^2 defects as well as high surface coverage of oxidized terminations [32] or submicron scale heterogeneity[25]. Concerning flat platinum, the poor quality of the signal could be linked to the fact that the electrode surface was not activated prior to the voltammetry analysis. The absence of electrochemical response on rough platinum electrode despite electrochemical activation is more puzzling. Therefore, we decided to go one step further in the investigation with an EDX comparison between rough and flat platinum. These results are presented in the next section.

The cathodic Charge Storage Capacity (CSC) of the cyclic voltammetry is given by *[4] :*

$$CSC = -\frac{1}{v \cdot S_{CONTACT}} \int_{i<0} IdV \quad (1)$$

Where v is the voltage sweep rate (50 mV/s)

When we compared in Table 1 the CSC values, nanostructured BDD has a slightly higher CSC than rough platinum which can be attributed to the outstanding wider voltage window of diamond. For comparison, high charge injection materials, such as sputtered iridium oxide film, have a CSC of 23 mC/cm^2 [4]. But the reactivity of diamond in PBS is very limited compared to the oxidation processes of platinum and such an exploration in voltage can be dangerous for neurons.

g) Further SEM characterizations

With such spongy surface, rough platinum should have a higher capacitive current than flat

platinum which is surprisingly not the case from the cyclic voltammetry of Fig. 8-A. To understand this phenomenon, we decided to perform EDX comparison between the rough and the flat platinum, see Suppl. Fig. 2.

This EDX comparison highlights the marked presence of Sulphur at the rough platinum surface. As the adsorption of Sulphur dioxide is known to poison the platinum surface [22], this could explain why the CSC of the rough platinum is nearly similar to the flat one.

h) Long term biocompatibility evaluation

In our study, passive devices were developed and implanted in a mini-pig for three months. Histological examinations were carried out post-mortem, 12 weeks after implantation, for the mini-pig. After euthanasia of the animal and removing skin and muscles covering the implant, observation of the implantation sites showed a thickening of the sutured dura mater in front of the craniotomy frame (Fig. 10-A) in comparison with the constitutive dura mater.

The end-stage healing response for biomaterials is generally fibrous encapsulation. In the current study, devices implanted below mini-pig dura mater were found to be encapsulated. An explanation of the presence of fibrous encapsulation may be due to the fact that the dura mater was injured during surgery and thus meningeal fibroblasts were activated, see Fig. 11. The presence of a translucent and thin (approximately 40 µm) neoformed tissue confirmed by microscopic examination explains the thickening of dura mater (Fig. 10-A, B).

The adhesion of the neoformed tissue with the cortical surface below and the dura mater above was also tested and we observed focal adhesions between the tissue capsule, the dura mater and the brain cortex (Fig. 10-A), without any macroscopic sign of tissue defect. Moreover, we observed that the neoformed tissue was not vascularized. This data suggests that the device can be easily explanted by the neurosurgeon.

As shown in Fig. 10-D, the cortical surface was modified by the implant and the MEA imprint is delimited by a dashed line.

The final study of the histological investigations was conducted to evaluate the brain cortex reaction beneath the MEA and to detect signs of inflammation. Firstly, Perls' iron staining was performed to detect signs of alteration and hemorrhaging due to the surgery. The macroscopic observations of the meninges and the brain cortex, surrounding the MEAs, revealed no histopathological changes by comparison with the control tissue (data not shown). The result suggests an absence of vascular damage around the implant.

We noted that expression of the astrocyte marker is highly increased in the glia limitans of brain cortex for the four conditions. The increase of the uncovered-glia limitans' thickness (surgical control) was because of the sutured dura pressure on the brain cortex (Fig. 11-A). In the MEAs-covered brain cortex, the glia limitans is continuous as shown in Fig. 11-B and Fig. 11-C. The GFAP staining is consistent and most astrocytes in the GFAP-intensive area were stellate in appearance. However, some astrocytes appeared hypertrophic in tissue beneath the Platinum/iridium multielectrode array.

Representative patterns of cortical Iba-1 expression in multielectrode array-covered and uncovered brain cortex areas are shown in Suppl. Fig. 3. The Immunostaining raised against the protein Iba-1 (Ionized calcium-binding adapt molecule 1 expressed by microglia and macrophages) showed the absence of activated microglial cells within the surgical control, the BDD and silicone MEA-covered brain cortex, after 12 weeks (Suppl. Fig. 3-A). The observation of the Platinum/Iridium MEA-covered brain cortex showed the presence of some activated microglial cells under the glia limitans (Suppl. Fig. 3-C).

Nevertheless, the leads' mechanical stiffness and volume should be decreased in the next version to avoid the device's mechanical stress on the brain, as the grid is placed subdurally. This is a possible explanation to the second impedance increase noticeable in Fig. 4 after 60 days. Considering the footprint of the implant in the brain, see Fig. 10-D, we should also decrease the overall implant's thickness (from 0.7 mm to less than 0.2 mm). The thickness of the grid was chosen from the standard ECoG grids (see Adtech, PMT Corp or Dixi) and the MEA mechanical stiffness possibly impaired the biological assessment of the materials.

The impedance evolution was significant on Fig. 3-C and Fig. 4, but considering the limited number of animals, it is unclear whether the impedance evolution is related to the ***mechanical mismatch*** of the MEA and its cables or to the contact material. It is often difficult to disassociate the roughness of the contact from the material itself. Most studies compare different materials with their specific deposition process in PBS: bowl-hat and rough platinum in our case, flat and grass platinum (Boehler et al., 2015). This is a major limitation of most in-vivo studies, including this one. Additionally, Meijs published a comparison between flat and porous titanium nitride in-vivo (with a rodent model), showing that protein diffusion was reduced on porous surfaces [33].

3. Conclusions

We described a functional biological assessment of BDD recording contacts. We remained as close as possible to an industrial process and compared the BDD to platinum iridium contacts optimized in terms of roughness. The nanostructured boron doped diamond-coating withstood the electrical welding and integration in the silicone rubber. Thus, the end result is a MEA comprised of medical grade materials, using industrial processes. With regard to the different steps of dicing, welding, and embedding in the insulator, the manufacturing process is remarkably reproducible and produces consistent impedance curves. The specific dicing process increased the roughness of the platinum iridium contacts compared to the bowl-hat shape (embossed Platinum iridium foil), hence a higher effective surface of the platinum contact.

Even if these results are limited in terms of statistical relevance, we may conclude that these BDD contacts are suitable for chronic implantation and this study confirmed the predominant role of contact roughness for recording. After three months in-vivo, the BDD contacts are stable and biocompatible. When compared to platinum iridium, the gold standard of active implantable devices, the evolution of tissue response or electrochemical impedance was comparable. We highlighted in-vivo a slight advantage for the rough platinum in terms of impedance. Whereas in PBS, the BDD has a slightly higher Charge Storage Capacity than rough platinum iridium electrodes.

Acknowledgements

The project was funded by European Community's Seventh Framework Program (FP7) under grant agreement n° 280433 (NEUROCARE project).

Christophe LEMONIAS from CEA performed the SEM and EDX characterizations.

References

[1] M. Alcaide, A. Taylor, M. Fjorback, V. Zachar, and C. P. Pennisi, “Boron-Doped Nanocrystalline Diamond Electrodes for Neural Interfaces: In vivo Biocompatibility Evaluation,” *Front. Neurosci.*, vol. 10, Mar. 2016.

[2] T. D. Y. Kozai, A. S. Jaquins-Gerstl, A. L. Vazquez, A. C. Michael, and X. T. Cui, “Brain Tissue Responses to Neural Implants Impact Signal Sensitivity and Intervention Strategies,” *ACS Chem. Neurosci.*, vol. 6, no. 1, pp. 48–67, Jan. 2015.

[3] D. R. Merrill, M. Bikson, and J. G. R. Jefferys, “Electrical stimulation of excitable tissue: design of efficacious and safe protocols,” *J. Neurosci. Methods*, vol. 141, no. 2, pp. 171–198, Feb. 2005.
[4] S. F. Cogan, “Neural Stimulation and Recording Electrodes,” *Annu. Rev. Biomed. Eng.*, vol. 10, no. 1, pp. 275–309, 2008.
[5] R. V. Shannon, “A model of safe levels for electrical stimulation,” *IEEE Trans. Biomed. Eng.*, vol. 39, no. 4, pp. 424–426, Apr. 1992.
[6] D. McCreery, V. Pikov, and P. R. Troyk, “Neuronal loss due to prolonged controlled-current stimulation with chronically implanted microelectrodes in the cat cerebral cortex,” *J. Neural Eng.*, vol. 7, no. 3, p. 036005, 2010.
[7] G. Piret *et al.*, “3D-nanostructured boron-doped diamond for microelectrode array neural interfacing,” *Biomaterials*, vol. 53, pp. 173–183, Jun. 2015.
[8] F. Sauter-Starace, O. Bibari, F. Berger, P. Caillat, and A. L. Benabid, “ECoG recordings of a non-human primate using carbon nanotubes electrodes on a flexible polyimide implant,” in *2009 4th International IEEE/EMBS Conference on Neural Engineering*, 2009, pp. 112–115.
[9] J. Liu *et al.*, “Stable non-covalent functionalisation of multi-walled carbon nanotubes by pyrene–polyethylene glycol through π–π stacking,” *New J Chem*, vol. 33, no. 5, pp. 1017–1024, 2009.
[10] J. Svítková, T. Ignat, Ľ. Švorc, J. Labuda, and J. Barek, “Chemical Modification of Boron-Doped Diamond Electrodes for Applications to Biosensors and Biosensing,” *Crit. Rev. Anal. Chem.*, vol. 46, no. 3, pp. 248–256, May 2016.
[11] M. Hupert *et al.*, “Conductive diamond thin-films in electrochemistry,” *Diam. Relat. Mater.*, vol. 12, no. 10–11, pp. 1940–1949, Oct. 2003.
[12] K. E. Bennet *et al.*, “Development of Conductive Boron-Doped Diamond Electrode: A microscopic, Spectroscopic, and Voltammetric Study,” *Materials*, vol. 6, no. 12, pp. 5726–5741, Dec. 2013.
[13] C. G. Specht, O. A. Williams, R. B. Jackman, and R. Schoepfer, “Ordered growth of neurons on diamond,” *Biomaterials*, vol. 25, no. 18, pp. 4073–4078, Aug. 2004.
[14] S. Kelly *et al.*, “Patterned growth of neuronal cells on modified diamond-like carbon substrates,” *Biomaterials*, vol. 29, no. 17, pp. 2573–2580, Jun. 2008.
[15] T. Lechleitner *et al.*, “The surface properties of nanocrystalline diamond and nanoparticulate diamond powder and their suitability as cell growth support surfaces,” *Biomaterials*, vol. 29, no. 32, pp. 4275–4284, Nov. 2008.
[16] Y.-C. Chen *et al.*, “The effect of ultra-nanocrystalline diamond films on the proliferation and differentiation of neural stem cells,” *Biomaterials*, vol. 30, no. 20, pp. 3428–3435, Jul. 2009.
[17] R. Kiran, E. Scorsone, P. Mailley, and P. Bergonzo, “Quasi-Real Time Quantification of Uric Acid in Urine Using Boron Doped Diamond Microelectrode with in Situ Cleaning,” *Anal. Chem.*, vol. 84, no. 23, pp. 10207–10213, Dec. 2012.
[18] R. J. Edgington *et al.*, “Patterned neuronal networks using nanodiamonds and the effect of varying nanodiamond properties on neuronal adhesion and outgrowth,” *J. Neural Eng.*, vol. 10, no. 5, p. 056022, 2013.
[19] A. Grill, “Diamond-like carbon coatings as biocompatible materials—an overview,” *Diam. Relat. Mater.*, vol. 12, no. 2, pp. 166–170, 2003.
[20] L. Tang, C. Tsai, W. W. Gerberich, L. Kruckeberg, and D. R. Kania, “Biocompatibility of chemical-vapour-deposited diamond,” *Biomaterials*, vol. 16, no. 6, pp. 483–488, Jan. 1995.

[21] C. S. Mestais, G. Charvet, F. Sauter-Starace, M. Foerster, D. Ratel, and A. L. Benabid, "WIMAGINE: wireless 64-channel ECoG recording implant for long term clinical applications.," *IEEE Trans. Neural Syst. Rehabil. Eng. Publ. IEEE Eng. Med. Biol. Soc.*, vol. 23, no. 1, pp. 10–21, Jan. 2015.
[22] M. M. Saleh, M. I. Awad, F. Kitamura, and T. Ohsaka, "Sulphur dioxide poisoning and recovery of platinum nanoparticles: effect of particle size," *Int J Electrochem Sci*, vol. 7, pp. 12004–12020, 2012.
[23] C. Hébert, J. P. Mazellier, E. Scorsone, M. Mermoux, and P. Bergonzo, "Boosting the electrochemical properties of diamond electrodes using carbon nanotube scaffolds," *Carbon*, vol. 71, pp. 27–33, May 2014.
[24] J. Bousquet, T. Klein, M. Solana, L. Saminadayar, C. Marcenat, and E. Bustarret, "Phase diagram of boron-doped diamond revisited by thickness-dependent transport studies," *Phys. Rev. B*, vol. 95, no. 16, p. 161301, Apr. 2017.
[25] K. Cinková, C. Batchelor-McAuley, M. Marton, M. Vojs, Ľ. Švorc, and R. G. Compton, "The activity of non-metallic boron-doped diamond electrodes with sub-micron scale heterogeneity and the role of the morphology of sp2 impurities," *Carbon*, vol. 110, pp. 148–154, Dec. 2016.
[26] M. Piangerelli *et al.*, "A fully integrated wireless system for intracranial direct cortical stimulation, real-time electrocorticography data transmission, and smart cage for wireless battery recharge," *Epilepsy*, vol. 5, p. 156, 2014.
[27] A. G. Zippo, P. Romanelli, N. R. Torres Martinez, G. C. Caramenti, A. L. Benabid, and G. E. M. Biella, "A novel wireless recording and stimulating multichannel epicortical grid for supplementing or enhancing the sensory-motor functions in monkey (Macaca fascicularis)," *Front. Syst. Neurosci.*, vol. 9, May 2015.
[28] C. Boehler, T. Stieglitz, and M. Asplund, "Nanostructured platinum grass enables superior impedance reduction for neural microelectrodes," *Biomaterials*, vol. 67, pp. 346–353, Oct. 2015.
[29] V. Sankar, E. Patrick, R. Dieme, J. C. Sanchez, A. Prasad, and T. Nishida, "Electrode impedance analysis of chronic tungsten microwire neural implants: understanding abiotic vs. biotic contributions," *Front. Neuroengineering*, vol. 7, May 2014.
[30] Ĺ. Švorc *et al.*, "Doping Level of Boron-Doped Diamond Electrodes Controls the Grafting Density of Functional Groups for DNA Assays," *ACS Appl. Mater. Interfaces*, vol. 7, no. 34, pp. 18949–18956, Sep. 2015.
[31] E. Vanhove, J. de Sanoit, P. Mailley, M.-A. Pinault, F. Jomard, and P. Bergonzo, "High reactivity and stability of diamond electrodes: The influence of the B-doping concentration," *Phys. Status Solidi A*, vol. 206, no. 9, pp. 2063–2069.
[32] E. Fortin *et al.*, "Interfacing Boron Doped Diamond and Biology: An Insight on Its Use for Bioanalytical Applications," *Electroanalysis*, vol. 17, no. 5–6, pp. 517–526, Mar. 2005.
[33] S. Meijs, C. Sørensen, S. Sørensen, K. Rechendorff, M. Fjorback, and N. J. M. Rijkhoff, "Comparison of the electrochemical properties of smooth and porous TiN electrode coatings in rats," in *2015 7th International IEEE/EMBS Conference on Neural Engineering (NER)*, 2015, pp. 486–489.
[34] H. A. Girard *et al.*, "Electrostatic grafting of diamond nanoparticles towards 3D diamond nanostructures," *Diam. Relat. Mater.*, vol. 23, pp. 83–87, Mar. 2012.

Supplementary data

a) Manufacturing of the BDD electrodes and integration in a silicone substrate

Prior to the growth, the disks were seeded with diamond nanoparticles using an electrostatic grafting technique already reported[34] and consisting in the sequential immersion of the disk in polydiallyldimethylammonium chloride (PDDAC from Sigma Aldrich), then in a solution of diamond nanoparticles (SYP GAF 0-0.05, Van Moppes®). The growth of the BDD layer was performed in a home-made Micro Wave Plasma Enhanced Chemical Vapor Deposition (MPCVD) reactor using CH_4, H_2 and TMB at a temperature between 450 and 500 ºC and a pressure of 20 Torr. These growth conditions are less aggressive compared to literature to avoid the high dilatation of metal inducing constrains as well as the use of promoting layer for the growth of diamond. Furthermore, low pressures allow the diffusion of the reactive carbon species inside the pores of the platinum iridium surface to induce a perfectly conformal coating.

Next, a 7 nm nickel catalyst layer was deposited onto the diamond surface via e-beam evaporation. The nickel film was turned into nickel nanoparticles of approximately 50 nm by dewetting at 700°C for 3 min (Schematic 1-3). The particle density was higher than 10^9 particles/cm^2. These particles were used as catalyst for the growth of Vertically-Aligned Carbon NanoTubes (VACNTs) in a PECVD ‘‘Black Magic’’ AIXTRON reactor. Very dense VACNTs with an average diameter of 50 nm were obtained with an average length of 2 µm (Schematic 1-4). The catalyst was removed using a two-step process. Firstly, the samples are placed in an Ultra High Vacuum oven and annealed at 900 ºC to sublimate the metal nanoparticle. Secondly, the samples are immersed in hot aqua regia solution for 5 min to eliminate any nickel residue (Schematic 1-5). Then a very dense electrostatic diamond nanoparticle coating of the CNTs is performed as reported in [23]. The high density of nanoparticle protects the CNTs from the plasma and allows a quick coalescence of the diamond particles. Finally the samples were placed in the same MPCVD reactor used for the first diamond layer to cover the CNTs with a 30 nm thick BDD (Schematic 1-6). As for the coating of the rough platinum-iridium surface, the growth of the diamond layer at the surface of the VACNTs was performed at low temperature and low pressure. The low pressure allows the diffusion of the carbon species to cover the VACNTs from the base to the top. As this coating is conformal the CNT surface is not accessible to fluids.

b) Animals and anesthesia and Surgery procedure

Two Yucatan mini-pigs identified A and B (approximately 12 kg) were premedicated with Stresnil® (Azaperone, Elanco, Lilly France) (2 mg/kg) intramuscularly (IM) and then anesthetized with Zoletil 100® (50 mg/mL tilétamine, 50 mg/mL zolazepam 10 mg/kg IM, Virbac, France). Following endotracheal intubation for the surgery, ventilation and anesthesia (Isoflurane 2% in carrier gas, Isoflo 100%®, Axience SAS) were provided by a volume-controlled ventilator (veterinary multipurpose ventilator MATRX Medical Inc. by TEM SEGA, France) in spontaneous respiratory mode. Fluid requirements were substituted with Ringer Lactate® solution (Lavoisier) intravenously and pain was controlled by using an analgesic agent (Vetergesic®, buprenorphine, 10 µg/kg IM, Sogeval, France). ECG, body temperature and oxygen saturation were monitored continuously. The mini-pigs eyes were protected by Lacrigel® (Europhta, Monaco). Prophylactic antibiotics (Duphamox LA, Zoetis, France SAS, amoxicillin, 15 mg/kg, IM) were also administered.

A midline skin incision was made from the animal's ears to the exposure of the Bregma. Since the Yucatan mini-pigs have a frontal sinus covering part of this zone (pneumatization), the craniotomies had to be performed in two steps. Firstly a bilateral rectangular craniotomy of the external table was done, followed by the same on the internal table. The paranasal frontal sinus in the anterior-lateral border of the craniotomies was exposed and irrigated using Betadine® (Povidone 12%, Meda Pharma France), sodium chloride 0.9% (NaCl) and oxygenated water 10 volume (H_2O_2, Cooper) to avoid contamination from the opened paranasal sinus. The dura mater was then carefully lifted with a sharp hook at the lateral side and incised.

For this in-vivo analysis, we implanted two electrode arrays (Fig. 1) over each sensorimotor cortex (see Suppl. Fig. 1) and biological controls in cortical areas that were not affected by the surgical procedure. This was done to avoid confounding surgical lesions, we had to identify responsive motor areas using an INOMED cortical stimulator (INOMED ISIS Iom and OSIRIS Neurostimulator©, Emmendingen, Germany). After closing the dura mater, bone flaps were fixed with titanium screws and plates (DePuy Synthes©) and covered with methyl methacrylate cement (Methax, Generique International, France). Mini-pig B was implanted for a three-month biocompatibility study with MEAs, without a connector. At the end of surgery for mini-pig A, the surgery differed by the subcutaneous tunnelization of two cables going from the MEA to a chronic percutaneous, at shoulder blade level. At the end of the procedure, to test the electrodes

functionality, a 5 min ECoG recording (Micromed© system, Micromed SD64, Micromed, Italy) and impedance spectrometry were performed on both hemispheres to compare BDD and PtIr contacts.

c) Electrochemical Impedance Spectroscopy and cyclic voltammetry prior to implantation

Both characterizations are performed using SP200 Potentiostat (Bio-Logic©, Seyssinet-Pariset, France). We used a set-up with two electrodes for the EIS: the reference and the counter electrode are both connected to the same platinum wire (0.5 mm in diameter) whereas we added a third electrodes to control the reference potential of the solution with a Ag/AgCl disk.

To evaluate the electrochemical behavior of the three materials and have a glimpse of their ability for electrical stimulation, we used cyclic voltammetry to characterize in three different conditions: (a) in aqueous sulfuric acid medium (pH1) (b) in PBS 1X (diluted solution from PBS 10X, Sigma Aldrich, France reference P5493), (c) in PBS containing a ferri-ferrocyanide probe (4 mM) sweep scan was set to 50 mV/s. The condition (a) enables the characterization of the platinum reactivity according to the reduction of protons, whereas condition (b) enables the assessment of the Cathodic Charge Storage Capacity (CSC), eventually in condition (c) the ferri-ferro cyanide probe enables the characterization of the electron transfer behavior of the different materials.

d) Scanning Electron microscopy

To image the nanostructures prior and after implantation, we used a SEM model H-4100 from Hitachi (Tokyo, Japan). After explantation, some samples were rinsed in PBS and dehydrated stepwise with ethanol (10 min for concentration 70°, 80°, 90° and then 20 min for 96°). Then the samples are dipped in HMDS for 5 min and dried during 3 min under aspiration. For further assessment of the platinum surface, we used a SEM model ULTRA PLUS from Carl Zeiss Microscopy GmbH (Jena, Germany) combined to the XFlash® detector 5030 and Esprit© software from Brücker (Mannheim, Germany) to identify the atoms of the surface.

e) Electrochemical Impedance Spectroscopy follow up during implantation

To check the grid efficiency for cortical recordings, impedance spectroscopy (6 electrodes placed over right hemisphere and 6 in the left) were performed during 3 months after surgery. A sampling rate of 1024 Hz (@16bit) was used for the grid recordings. Data was acquired under general anesthesia and using a SP200 Potentiostat with a two electrode set-up. One electrode of

the Electrode arrays was set as counter and reference electrode. Once a week, the impedance was recorded for each contact in the frequency range 1 Hz to 1 MHz, amplitude of the sinusoidal voltage is 50 mV.

f) Cortical activity recording (ECoG)

The ECoG signals were recorded throughout an electronic board to MicroMED® 64 channels set-up. The signal was recorded with a sampling rate of 1024 Hz on [0.1 Hz; 500 Hz] bandwidth and magnified 1000 fold for electrophysiological recordings.

Data were later analyzed using Micromed software System Plus® and noise computations programmed on Matlab®.

The Power Spectrum Densities are computed for week 1 and week 12 in Fig. 5. Areas highlighted in yellow represents frequencies with a significant difference ($p<0.001$) between power in Pt and BDD recordings (RMANOVA corrected for multiple comparison-Bonferroni post-test).

g) Tissue preparation and histological analysis of brain reactivity

Three months after implantation, the mini-pig B was perfused transcardially with 0.9% NaCl followed by 10% Neutral Buffered Formalin (Sigma Aldrich, France, reference HT501128-4l). After fixation, the brain including the samples was then removed and post-fixed overnight in the same fixative. The samples were carefully removed for electron microscopy analysis and tissue response around and under samples were performed. Next, the brain was placed in phosphate-buffered saline (PBS) with the addition of 30% sucrose until the block sank. Before freezing, the brain was cut to form blocks and brain blocks were then sectioned coronally and serially using a freezing microtome. Sections were collected and were processed for Nissl and Masson's Trichrome staining and immunohistochemistries for glial fibrillary acidic protein (GFAP), Ionized calcium-binding adapt molecule 1 (Iba1). Sections were incubated with the following primary antibody solutions overnight at 4°C including: anti-GFAP (1:500, polyclonal rabbit IgG, Dakocytomation, Glostrup, Denmark) to identify astrocytes, anti-Iba1 (1/500, polyclonal rabbit IgG, Wako Chemicals GmbH, Neuss, Germany) to identify macrophage/microglia. Secondary antibodies (Molecular Probes) were diluted for GFAP and Iba1. All sections were counterstained by incubation with the nuclear dye Propidium Iodide (Sigma Aldrich). Sections treated only with secondary antibody but with no primary antibody were used to determine non-specific binding. Tissue sections were mounted with Fluorsave reagent (Merck Millipore, France) and bound

primary antibodies were visualized on a set of slices arbitrary defined using a confocal microscope.

Figures

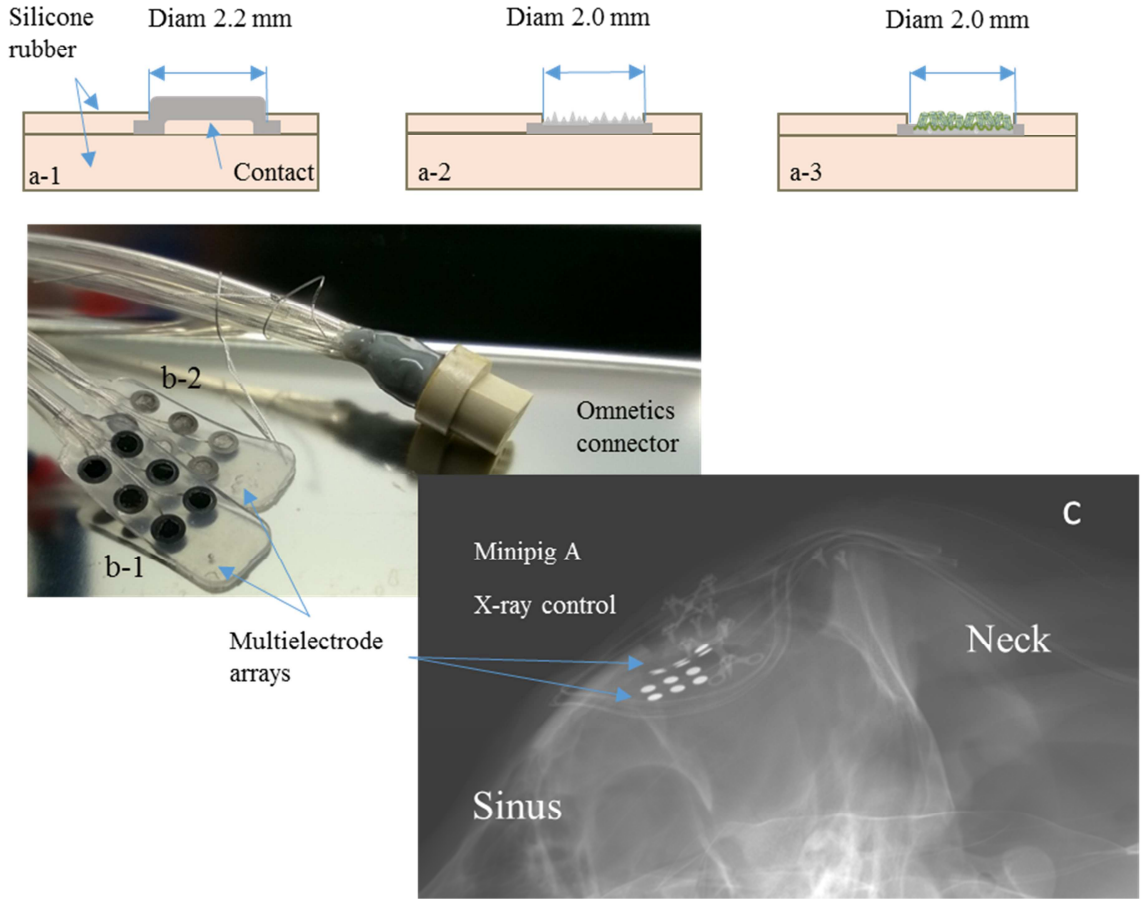

Fig. 1: (a) Schematic cross section of the different Multi-Electrodes Arrays. (a-1) Bowl-hat platinum contacts, (a-2) Rough platinum contacts, (a-3) Rough platinum contacts coated by 3D nanostructured boron. (b) Assembly of the BDD (b-1) and PtIr (b-2) MEA with the micro-circular Omnetics connector. (c): X Ray control after implantation.

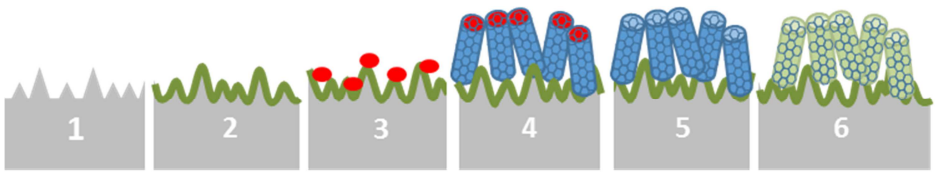

Schematic 1: Processing the nanostructured boron doped diamond (BDD) on rough platinum iridium disks. 1: rough dicing of the platinum rod, 2: nanoseeding of BDD, 3: creation of the nanobeads of Nickel catalyst, 4: carbon nanotube growth; 5: dissolution of the catalyst, 6: BDD deposition over the CNTs

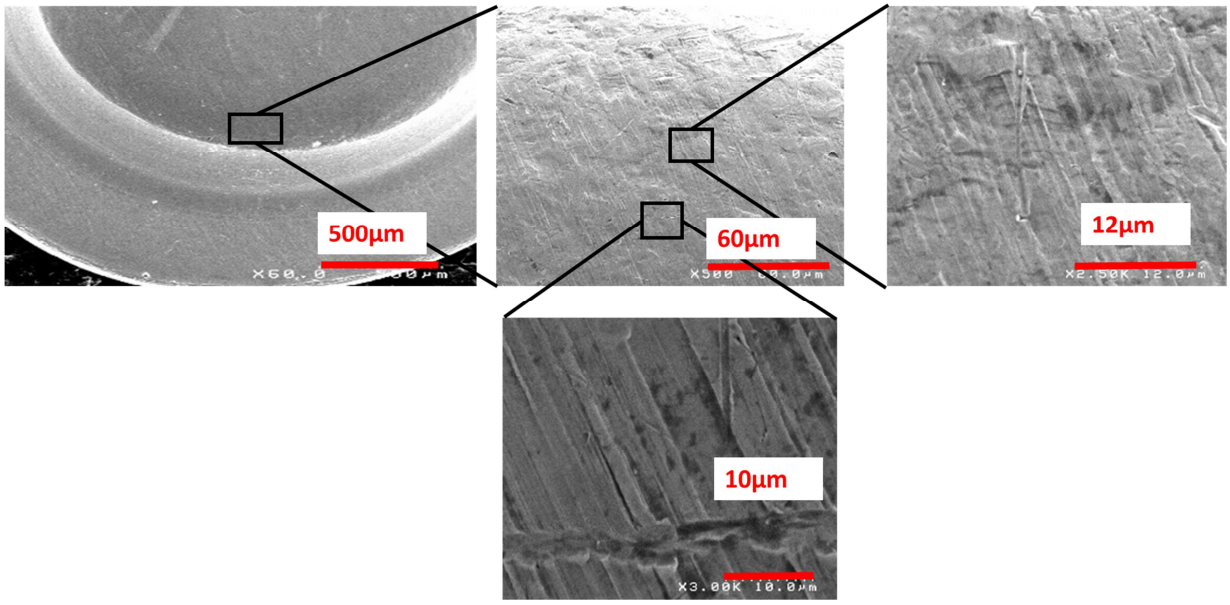

Fig. 2 : SEM of the bowl-hat platinum iridium contact

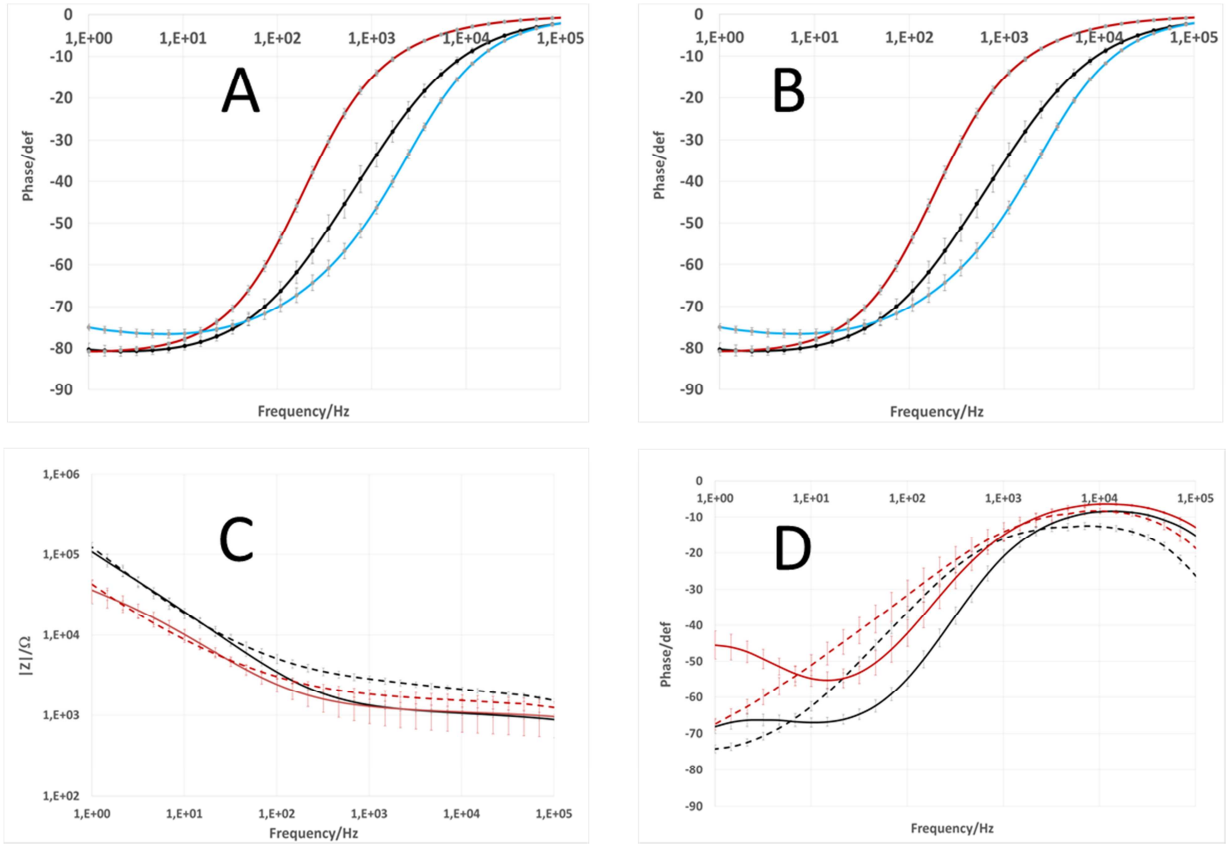

Fig. 3 : Impedance modulus (A) and phase (B) of electrodes in PBS, mean and standard error on 12 contacts of each type. Follow up first week (1W, solid line) and 12th week (12 W, dashed line) after implantation for Platinum iridium (red), Boron-Doped Diamond (black), impedance modulus (C) and Phase (D)

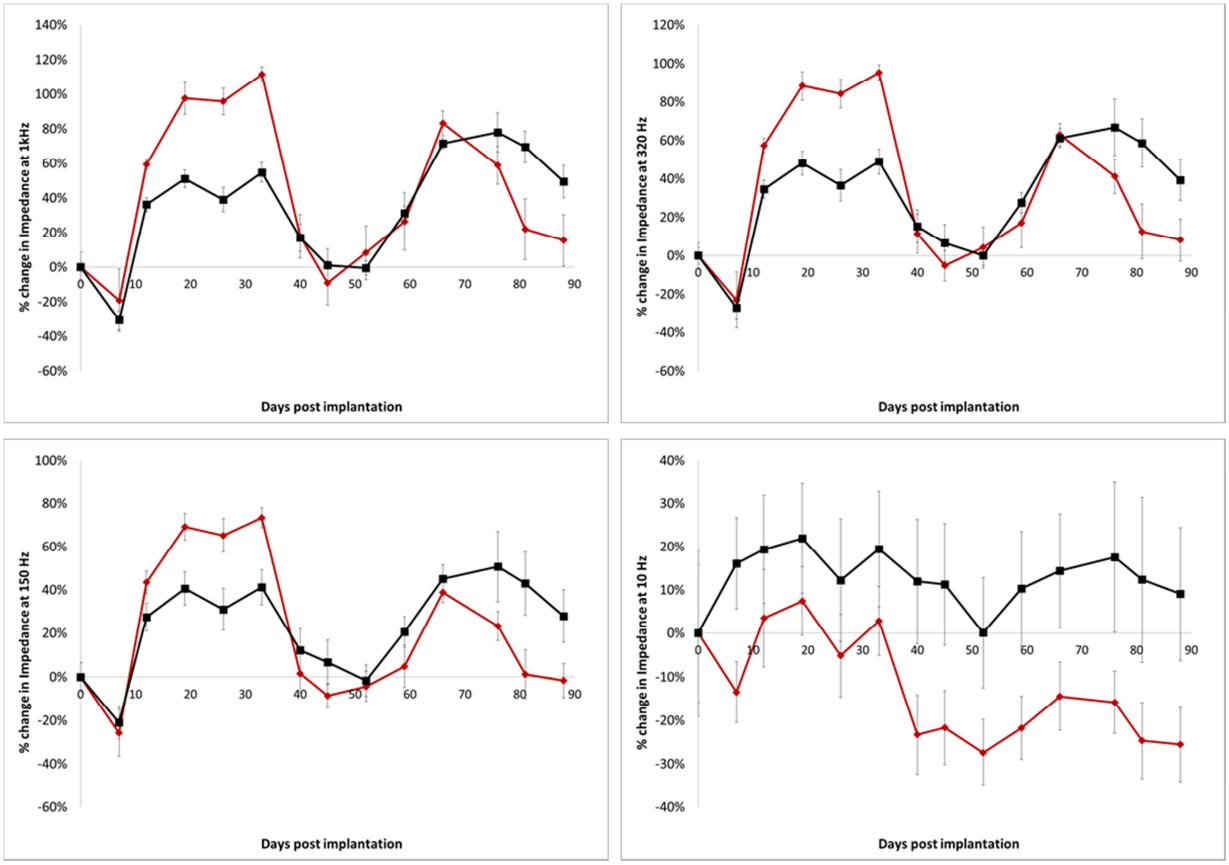

Fig. 4 : Relative change of In vivo impedance measured at 10; 150; 320; 1000 Hz. Platinum contacts are plotted in red and BDD in black. Error bars stand for the standard error.

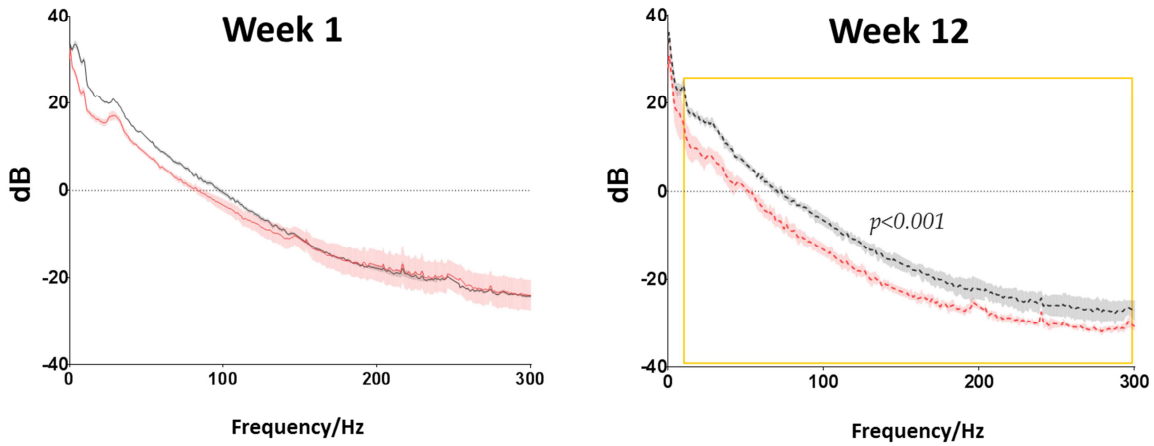

Fig. 5 : ECoG-Power Spectrum Density (with 50 Hz notch filter). Averaged power spectra densities were calculated across 5 ECoG Rough platinum (Pt) or Boron Doped Diamond (BDD) contacts, evenly distributed in the frontal cortex. Pt electrodes are represented in red and BDD in black. Background colors indicate the standard error. Box highlighted in yellow represents frequencies with a significant difference ($p<0.001$) between power in Pt and BDD recordings (RMANOVA corrected for multiple comparison-Bonferroni post-test).

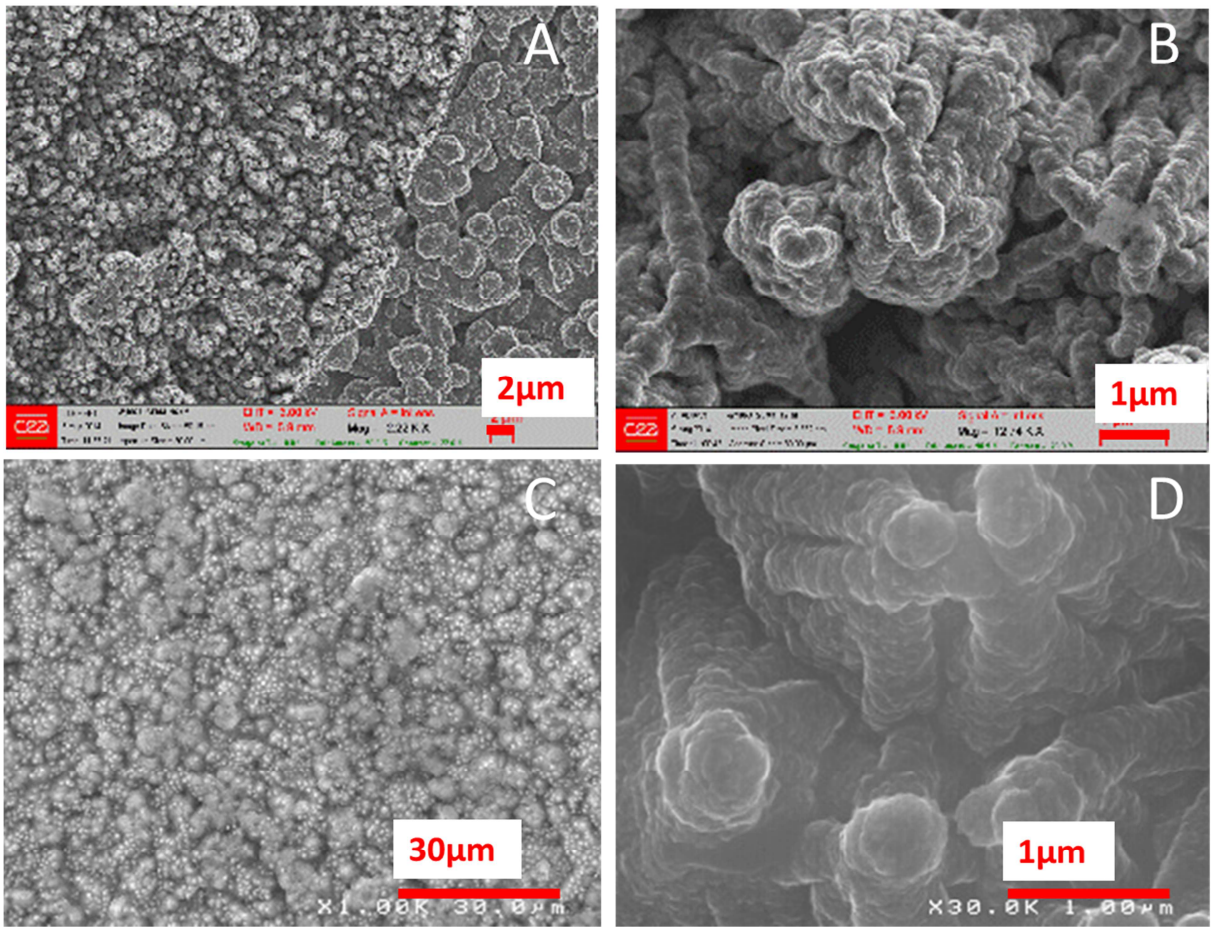

Fig. 6 : SEM of Boron Doped Diamond contacts. (A, B) Prior to implantation. (C, D) After 12 week implantation.

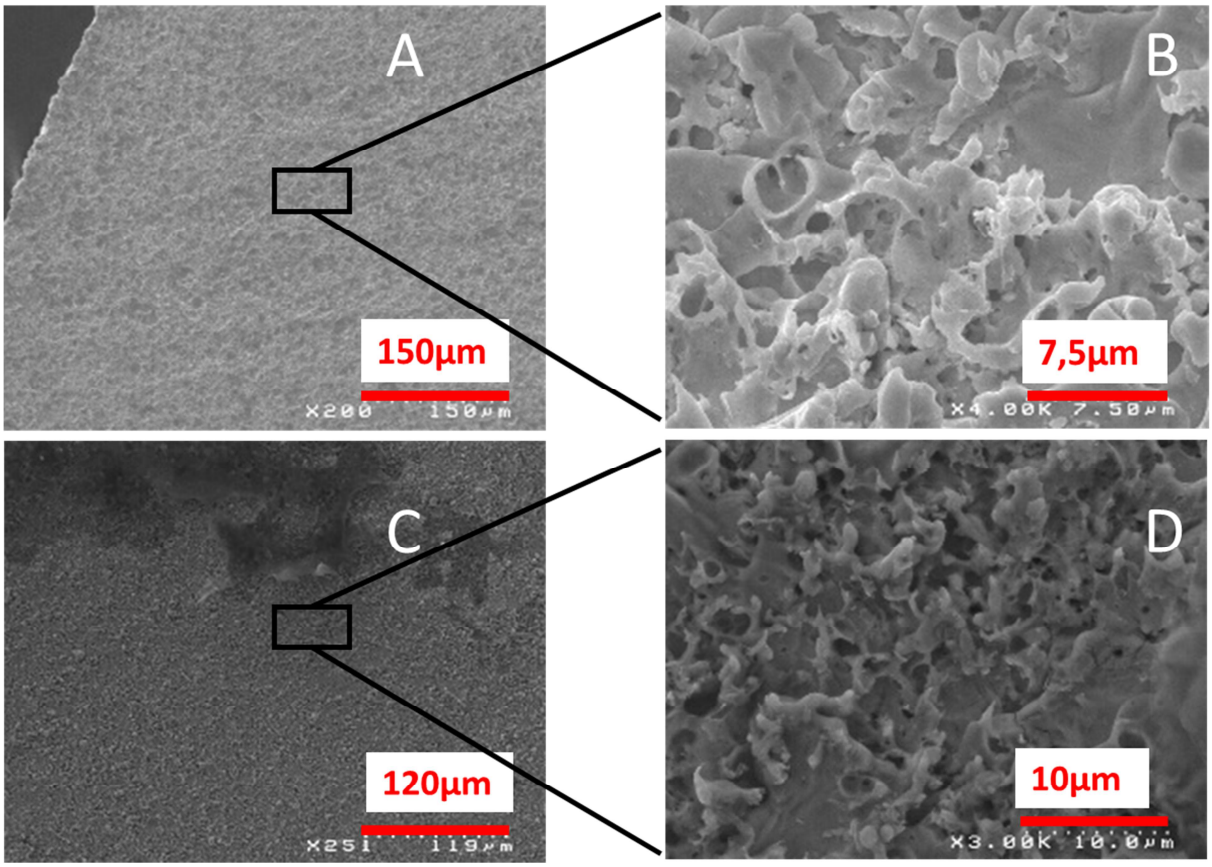

Fig. 7 : SEM of nanostructured platinum iridium contacts, (A, B) prior to implantation. (C, D) after 12 Week implantation

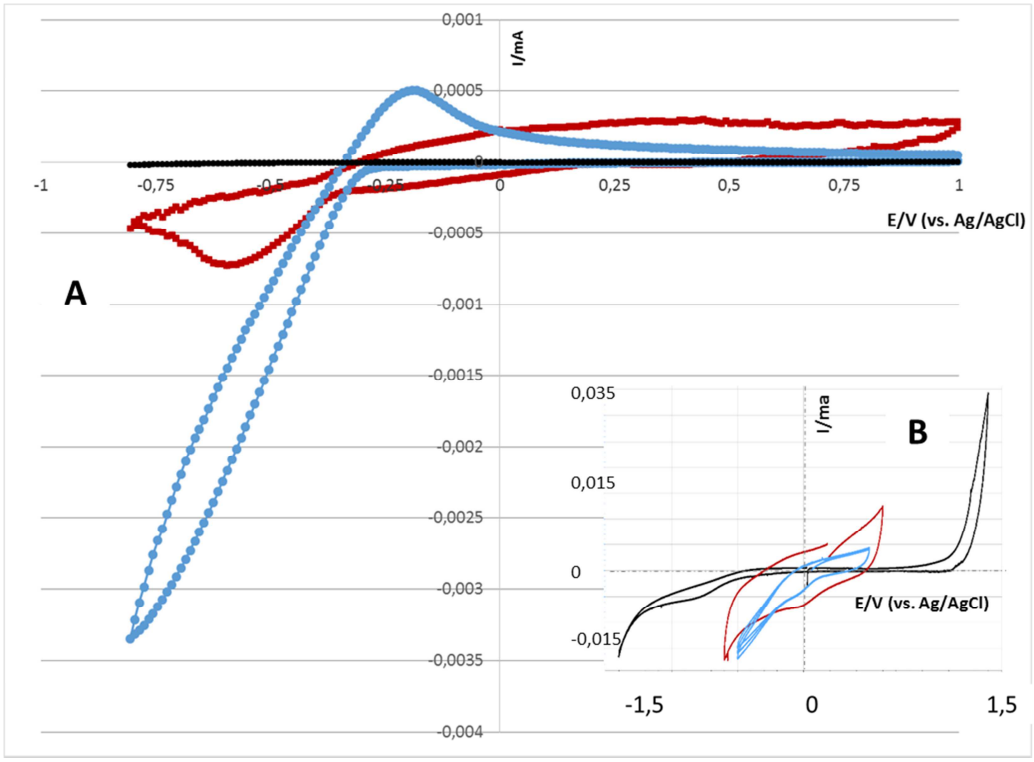

Fig. 8 : (A) Cyclic voltammetry of contacts in sulfuric acid aqueous bath (pH 1), (B) in PBS 1X. Nanostructured BDD (black), Flat Platinum (blue), Rough platinum (red).

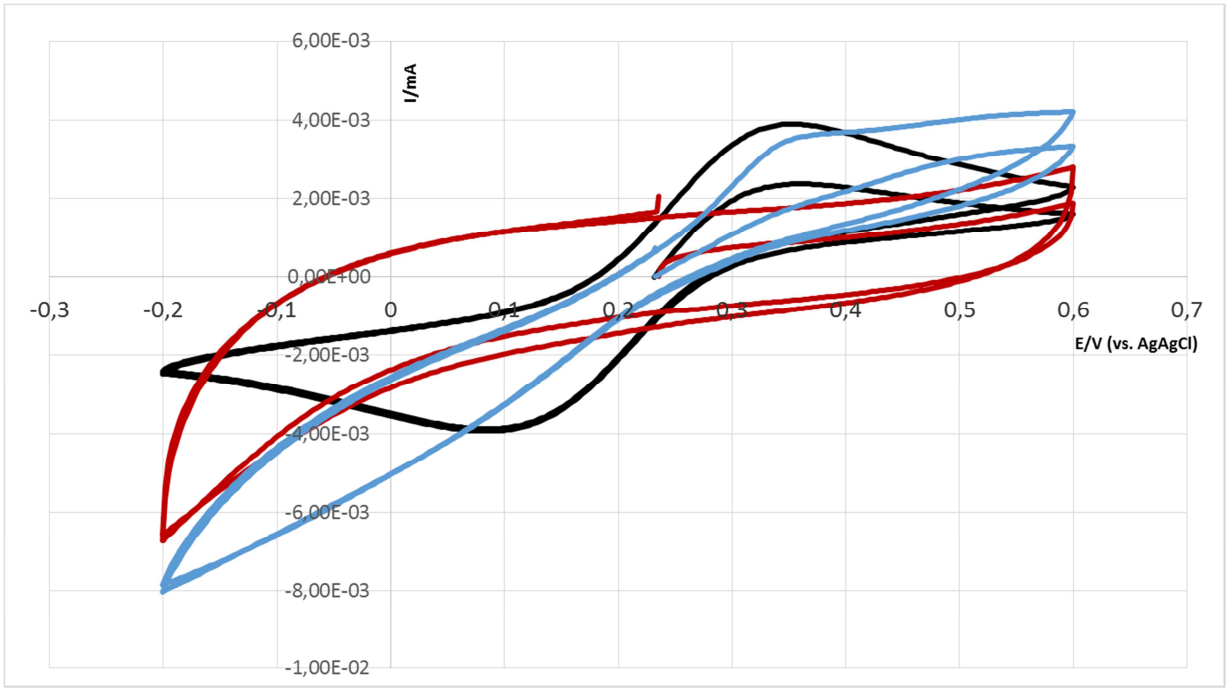

Fig. 9 : Cyclic voltammetry in PBS+4mM ferri-ferrocyanide. Nanostructured BDD (black), flat platinum (blue), Rough platinum (red).

Contact materials	Flat platinum iridium	Rough platinum iridium	Boron Doped Diamond
CSC (in mC/cm^2)	4.32	5.38	6.26

Table 1: cathodic Charge Storage Capacity in PBS

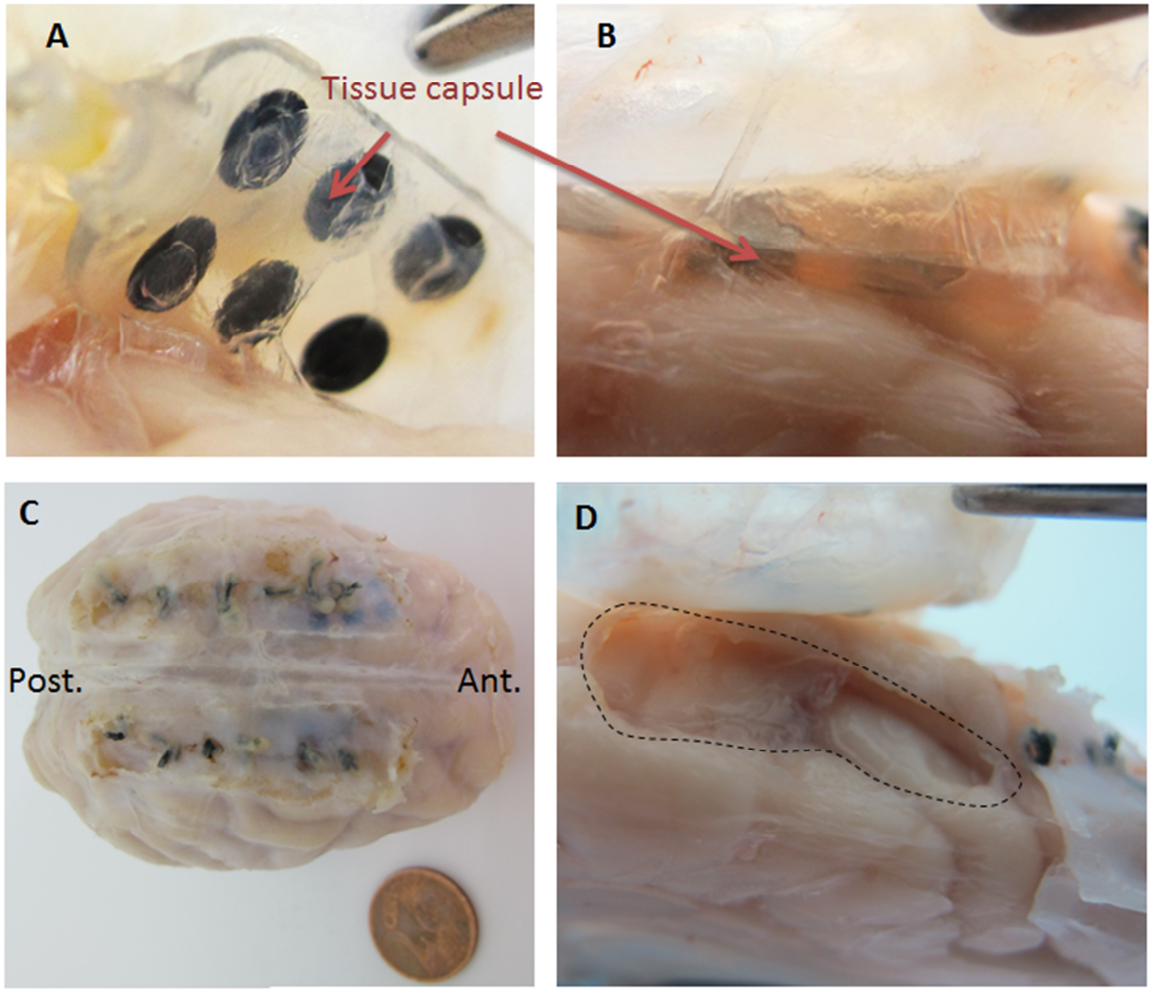

Fig. 10 : A – Multielectrode array with Diamond electrodes after 12 weeks, embedded in a neoformed tissue. B – Platinum iridium contacts after 12 weeks, embedded in a reactive tissue. C – The mini-pig (B) brain with the dura mater after 12 weeks of contact with the multielectrode arrays. D –rough platinum/ iridium-MEA-covered brain cortex.

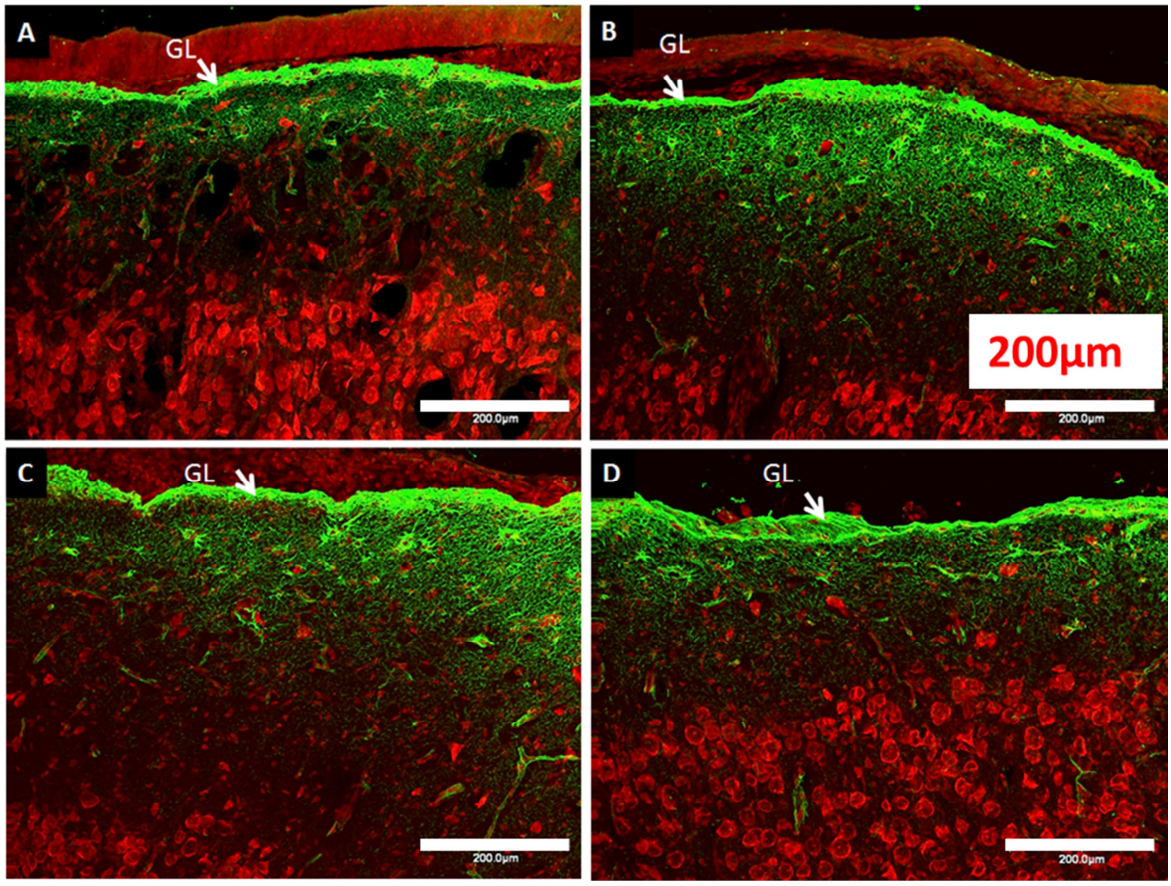

Fig. 11: Representative glial fibrillary acidic protein (GFAP) expression patterns in uncovered-brain cortex (surgical control) (A), in diamond-MEA-covered brain cortex (B), in iridium/rough platinum-MEA-covered brain cortex(C) and in silicone-covered brain cortex (D). Scale bar = 200 µm. GL: glia limitans.

Supplementary figures

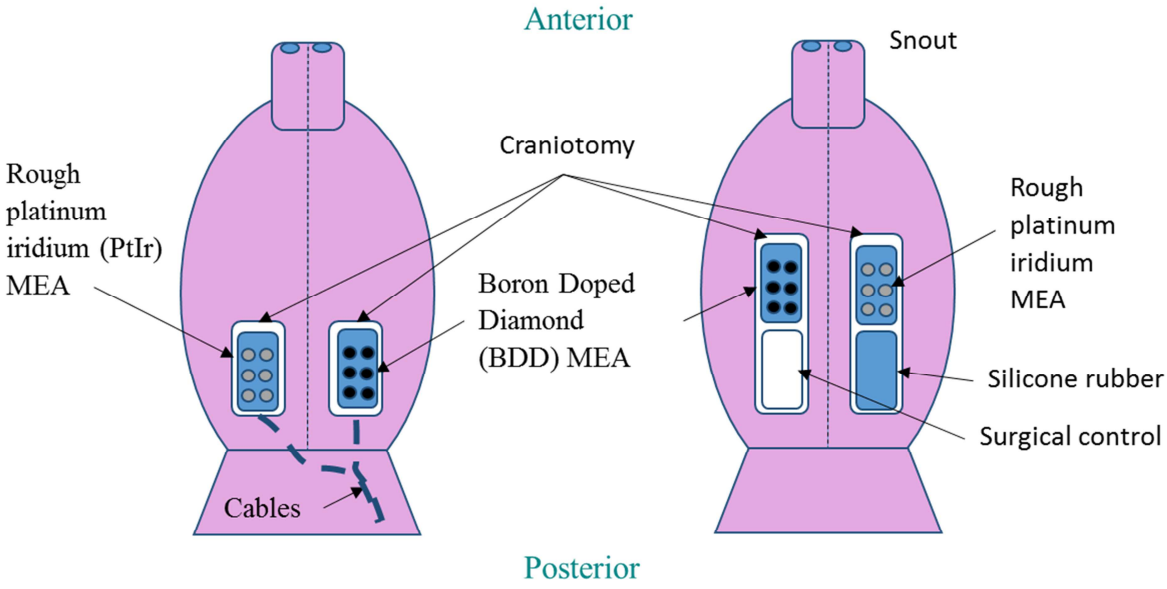

Suppl. Fig. 1 : Implantation schematic of the mini-pigs. (Left) mini-pig A, (right) mini-pig B

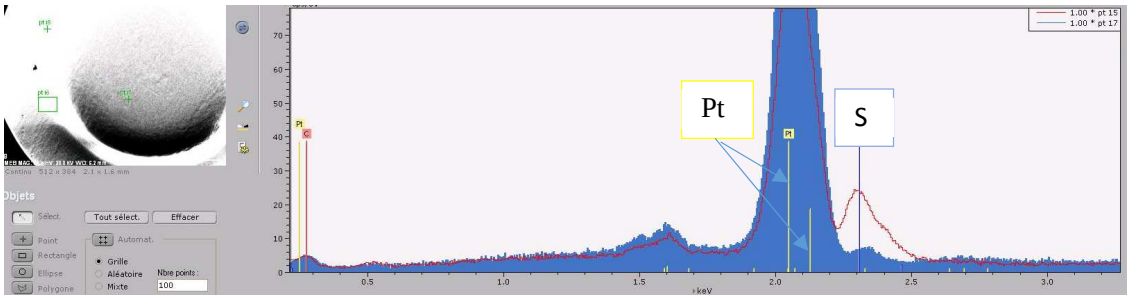

Suppl. Fig. 2 : On the left SEM picture of the flat platinum, on the right EDX of PtIr rough (red) vs. flat (blue filled)

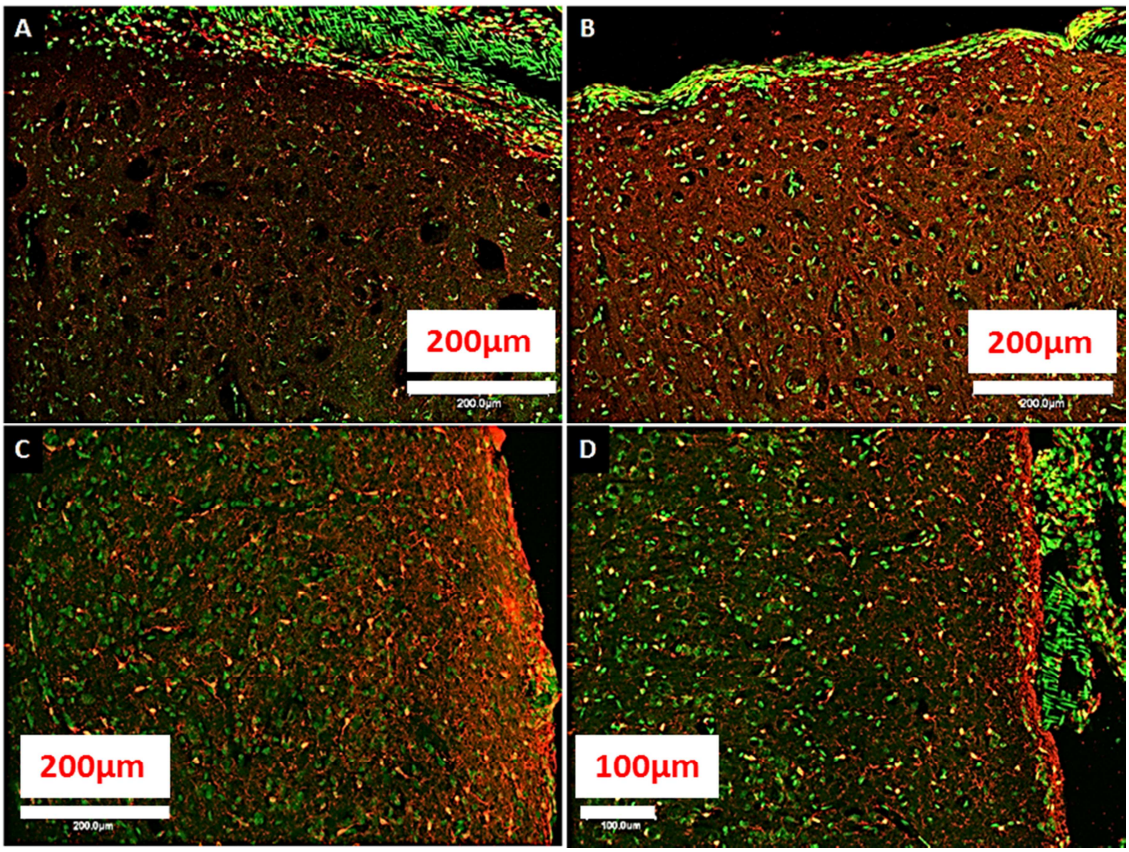

Suppl. Fig. 3 : Representative ion calcium binding adaptor molecule 1 (Iba-1) expression patterns in uncovered-brain cortex (surgical control) (A), in diamond-MEA-covered brain cortex (B), in iridium/rough platinum-MEA-covered brain cortex(C) and in silicone-covered brain cortex (D).